

pubs.acs.org/JPCL Letter

Dynamic Ligand Surface Chemistry of Excited PbS Quantum Dots

Eric R. Kennehan, Kyle T. Munson, Grayson S. Doucette, Ashley R. Marshall, Matthew C. Beard, and John B. Asbury*



Cite This: J. Phys. Chem. Lett. 2020, 11, 2291-2297



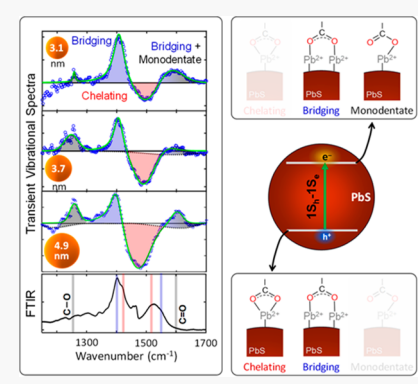
ACCESS

Metrics & More



SI Supporting Information

ABSTRACT: The ligand shell around colloidal quantum dots mediates the electron and energy transfer processes that underpin their use in optoelectronic and photocatalytic applications. Here, we show that the surface chemistry of carboxylate anchoring groups of oleate ligands passivating PbS quantum dots undergoes significant changes when the quantum dots are excited to their excitonic states. We directly probe the changes of surface chemistry using time-resolved mid-infrared spectroscopy that records the evolution of the vibrational frequencies of carboxylate groups following excitation of the electronic states. The data reveal a reduction of the Pb—O coordination of carboxylate anchoring groups to lead atoms at the quantum dot surfaces. The dynamic surface chemistry of the ligands may increase their surface mobility in the excited state and enhance the ability of molecular species to penetrate the ligand shell to undergo energy and charge transfer processes that depend sensitively on distance.



olloidal quantum dots (QDs) exhibit size-tunability and discrete electronic states with potential application in a variety of optoelectronic applications. For example, solar cells that utilize QDs as a light absorbing layer have the potential to overcome efficiency limitations of single junction solar cells through a number of mechanisms, including multijunction devices, multiplication of photocurrent via multiple exciton generation (MEG), or hot-carrier extraction before thermalization of photogenerated carriers is complete. The latter two processes benefit from the potential to slow the relaxation of excited electronic states that arises from an energy mismatch between the low frequency phonon modes of inorganic nanocrystals and the discrete energy gaps between electronic states of the quantum confined nanostructures.

This slowing of relaxation processes in such quantum confined structures is known as the phonon bottleneck. While the process has been challenging to observe in quantum dots of CdS and CdSe, 14-18 it has been observed in PbSe nanostructures with carefully tailored multishell structures. The absence of a phonon bottleneck in CdS and CdSe has been rationalized in terms of the difference in effective masses of electrons versus holes. This allows excess energy of electrons to transfer to holes via an Auger-type process followed by rapid relaxation through the more closely spaced electronic states of the holes. This subsequent relaxation process can be facilitated by coupling of the excitonic states to the vibrational modes of surface ligands. 19-21 Recent studies have provided further support for the coupling of ligand vibrations to excitonic states of CdSe QDs.²²⁻²⁶ The absence of the phonon bottleneck in PbS or PbSe nanostructures without carefully tailored multishell structures has been more challenging to explain.

We recently provided new insight about the role that electron—phonon coupling plays in creating resonant relaxation paths between quantum confined states of PbS quantum dots that provide clarity regarding this question.²⁷

The ability to extract multiple charges per photon from MEG or to harvest hot carriers before they relax in photovoltaic devices requires that electrons or holes transfer rapidly across ligand-nanocrystal boundaries.²⁸ Examples of such charge transfer processes include the use of nanocrystals as photoreceptors in photocatalytic systems in which redox shuttles such as viologens^{29,30} were used to extract charges from photoexcited QDs for transport to catalysts present in solution.31-33 In other examples, QDs acted as the redox photocatalyst where substrates could approach the QD surfaces and be oxidized or reduced followed by subsequent radical-radical reactions.^{34–38} Such charge transfer processes can be facilitated by penetration of the redox shuttles within the ligand shell. Ligands can also have a pronounced influence on the electronic states of QDs. ^{39–44} Variations of the highest occupied and lowest unoccupied orbitals of the nanocrystals were recently demonstrated over a 2 eV range, 43 indicating that PbS QDs may be used to drive charge transfer processes involved in both photocatalytic oxidation or reduction reactions depending on the choice of ligands. Furthermore,

Received: February 18, 2020 Accepted: March 4, 2020 Published: March 4, 2020



interesting and difficult chemical reactions can be photocatalyzed when the surface bound ligands themselves are the reagents. In this case, the surface/ligand interactions can be used to template for the final product.⁴⁵

Despite their important roles in QD photophysics and photocatalysis, ligand-nanoparticle interactions in the excited electronic states of QDs have been challenging to characterize directly through their transient vibrational spectra. Fortunately, recent advances in time-resolved mid-infrared (TRIR) spectroscopy have enabled investigations of how molecular structure influences the excited state electronic properties of optoelectronic materials. 27,46-50 Motivated by these studies, we used TRIR spectroscopy to examine changes of the ligand surface chemistry and bonding to nanocrystal surfaces of PbS QD films passivated with oleate ligands following optical excitation to excited electronic states. The transient vibrational spectra reveal changes of bonding of the carboxylate groups, indicating that the oleate ligands undergo significant structural perturbation upon photoexcitation. Because ligand-nanocrystal interfaces play a central role in charge transfer and photochemistry of quantum dots, 31,51 the ability to directly probe ligand surface chemistry during excited state processes may be used to gain a more complete description of how excited state dynamics of the ligand shell influences photocatalytic processes of such systems. 28-33,51

Carboxylates are common anchoring groups for ligands attached to lead chalcogenide nanocrystals. They are the surface-active functional group of oleate ligands used in the synthesis of PbS and PbSe^{52,53} and are also involved in bonding of smaller ligands such as mercaptopropionic acid used to enhance the electronic coupling of nanocrystals in quantum dot solids for optoelectronic and photovoltaic applications. 54,55 The bonding geometry of carboxylate groups to metal ions at surfaces or in coordination compounds has a significant influence on their carbon-oxygen stretching frequencies. In fact, the correlation between vibrational frequency and bonding geometry is sufficiently well-defined in carboxylate complexes and crystalline materials to enable their carboxylate-metal bonding geometries to be catalogued according to their carbon-oxygen stretch frequencies. Figure 1a illustrates three common bonding geometries that carboxylates can adopt when they interact with metals ions. The bridging and chelating geometries are characterized by symmetric ν_{sym} and antisymmetric ν_{as} stretch modes that differ in frequency by approximately $\Delta \nu = 150$ and 100 cm⁻¹, respectively. The unidentate bonding geometry possesses formal double-bonded C=O and single-bonded C-O moieties with a much larger frequency difference $\nu_{C=0}$ - $\nu_{\rm C-O}$ near $\Delta \nu = 300 \text{ cm}^{-1.56}$

Vibrational features corresponding to these bonding geometries appear in the Fourier transform infrared (FTIR) spectra of the oleate passivated PbS QD films examined here (Figure 1b). The films were cast in air from octane onto BaF₂ substrates coated with a thin mesoporous alumina adhering layer as reported previously.²⁷ Immediately after being deposited, the films were sealed in a cryostat under nitrogen atmosphere for all optical measurements. The diameters of the QDs were found to be 2.9, 3.1, 3.7, and 4.9 nm, determined by fitting the visible/near-infrared (vis/near-IR) absorption spectra and confirmed through high-resolution TEM images (Supporting Information). The FTIR spectra of films of different nanocrystal sizes are essentially indistinguishable. Therefore, we use the spectrum of the 2.9 nm PbS QD film to

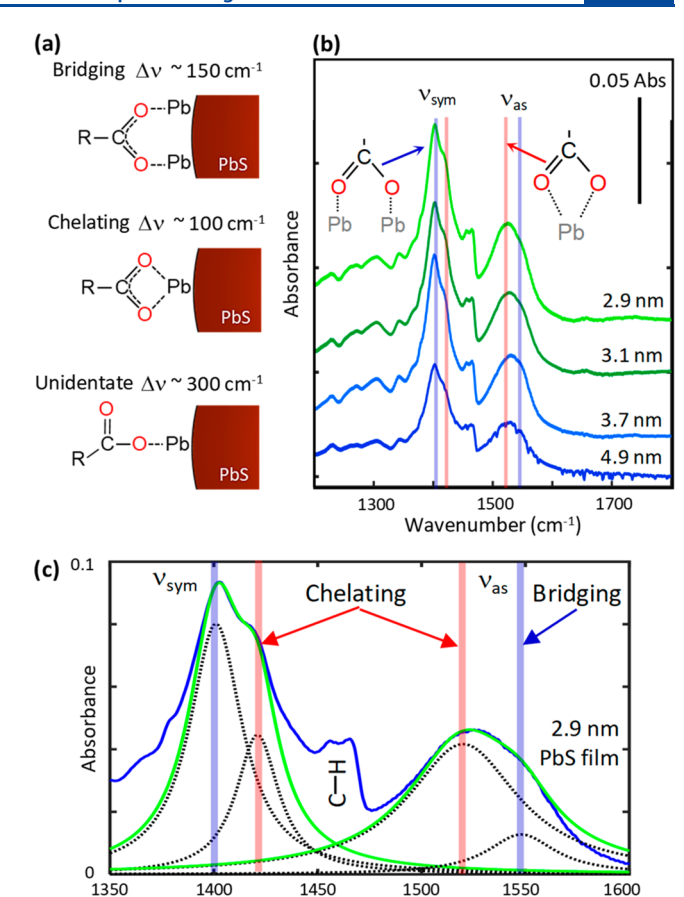


Figure 1. (a) Illustrations of common carboxylate binding motifs and the corresponding frequency differences of their carboxylate stretch modes. (b) FTIR spectra of four different size PbS QD films with oleate ligands. Distinct vibrational modes including symmetric $\nu_{\rm sym}$ and antisymmetric $\nu_{\rm as}$ carboxylate stretches are labeled with corresponding structures. (c) FTIR spectrum of 2.9 nm PbS QD film with Lorentzian fit functions used to identify the $\nu_{\rm sym}$ and $\nu_{\rm as}$ modes of the chelating (red) and bridging (blue) bonding geometries. These are marked by vertical lines that correspond to those appearing in panel b.

Wavenumber (cm⁻¹)

represent the FTIR spectra of all the samples in the discussion that follows.

Vertical lines in Figure 1b serve as guides to the eye highlighting the lower frequency symmetric ν_{sym} stretch of carboxylate groups around 1400-1420 cm⁻¹ and the higher frequency antisymmetric $\nu_{\rm as}$ stretch around 1520–1550 cm⁻¹. The spectra have been offset for clarity. Figure 1c depicts an expanded view of the spectrum of the 2.9 nm PbS QD film that is overlaid with Gaussian fit functions (dotted curves) used to identify the frequencies of the ν_{sym} and ν_{as} stretch modes of the bridging and chelating bonding geometries of oleate ligands in the film. The locations of the ν_{sym} and ν_{as} of chelating carboxylate groups at 1420 and 1520 cm⁻¹ and the bridging groups at 1400 and 1550 cm⁻¹ are consistent with prior studies of carboxylate binding motifs. ^{53,56} The long aliphatic chains of the oleate ligands contribute a C-H bend vibrational feature between the $\nu_{\rm sym}$ and $\nu_{\rm as}$ modes. FTIR spectra of other prominent vibrational modes including the aliphatic and alkene C-H stretch modes around 2900 cm⁻¹ appear in the Supporting Information. We note that the C=O stretch frequency of carboxylates bonding with the unidentate

geometry appear around 1600 cm⁻¹.⁵⁶ Therefore, the absence of a peak at 1600 cm⁻¹ in the FTIR spectra indicates that oleate ligands bond to PbS surfaces primarily through bridging and chelating geometries in the ground electronic states of the nanocrystals.

We investigated ligand—nanoparticle interactions between surface bonded oleate molecules and PbS QDS using TRIR spectroscopy in an effort to explore how the bonding interactions may change following photoexcitation to their excited electronic states. Transient absorption spectra measured between 1150 and 1800 cm⁻¹ in PbS QD films deposited from solutions of 2.9, 3.1, 3.7, and 4.9 nm diameter nanocrystals passivated with oleate ligands are represented in Figure 2a-d, respectively. The spectra were measured following

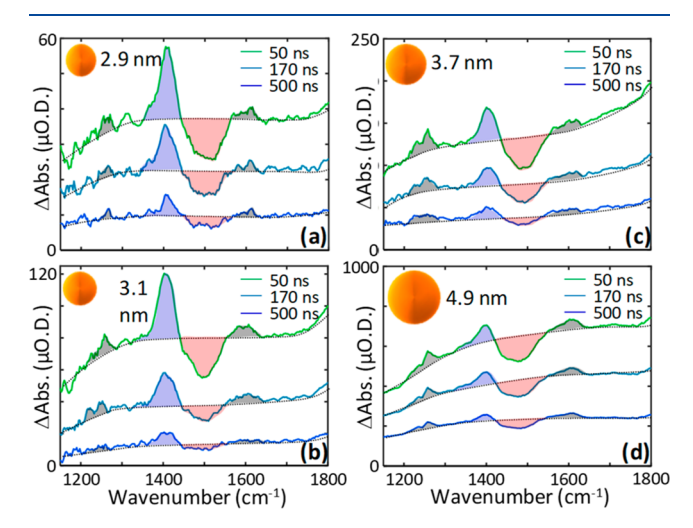


Figure 2. TRIR spectra measured at several delay times following 532 nm excitation of (a) 2.9 nm, (b) 3.1 nm, (c) 3.7 nm, and (d) 4.9 nm PbS QD films passivated with oleate ligands. The spectra consist of narrow vibrational features (shaded regions) that are superimposed on broad electronic features corresponding to the $1S_{e(h)}-1P_{e(h)}$ intraband transitions (dotted curves).

excitation at 532 nm with a 2 ns laser pulse with excitation intensity of 2 $\mu J/cm^2$. Given a density of QDs in the films of $\sim \! 10^{19}~cm^{-3}$, this corresponded to a density of absorbed photons of $<\! 0.02/QD$ even for films made from the largest 4.9 nm QDs. In all cases, the transient absorption spectra exhibit narrow vibrational features that are superimposed onto broad electronic absorptions that arise from the $1S_{e(h)}\! -\! 1P_{e(h)}$ intraband transitions of the PbS QDs. We note that we showed in our earlier publication that charge traps or defects contribute negligibly to the photophysics of the PbS QDs examined here. Therefore, the vibrational features represent perturbations of oleate ligands in the excitonic excited states of the QDs rather than due to defect states.

The narrow vibrational features introduce concave-up and concave-down curvature in the transient absorption spectra that indicate their locations by visual inspection of the data without further analysis. The vibrational features have been shaded for clarity in Figure 2 on the basis of this curvature. Nonetheless, we separated the transient vibrational features from the broad electronic transitions using the following fitting procedure from which we obtain the transient vibrational spectra of the PbS QD films represented in Figure 3a. To separate the features, we took the position that the electronic transitions would vary smoothly with frequency and adopted

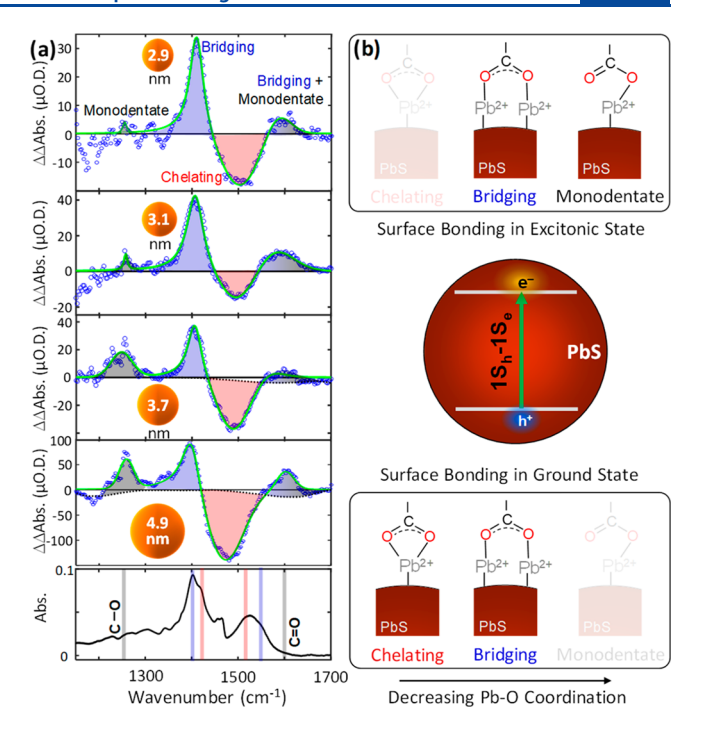


Figure 3. (a) Transient vibrational spectra of carboxylic groups anchored to PbS surfaces following 532 nm excitation of 2.9, 3.1, 3.7, and 4.9 nm PbS QD films passivated with oleate ligands. The ground state bleach feature overlaps the vibrational modes of chelating carboxylate groups appearing below in the spectrum of the 2.9 nm PbS QD film. Vibrational features of the excited excitonic state correspond to enhanced bridging and monodentate bonding geometries. (b) Cartoon depiction of the change in bonding from the ground to the excited excitonic states indicating a loss of the chelating and an increase of the monodentate geometries. These changes correspond to a decrease of the average Pb—O coordination in the excitonic excited state.

third order polynomial functions to fit their curvature in the 1150–1800 cm⁻¹ spectral window. This allowed us to fit the curvature of the electronic transitions at frequencies below 1200 cm⁻¹ and above 1650 cm⁻¹. This is important because this approach enabled us to estimate the shape of the electronic transitions using the frequency regions where the vibrational features do not appear so we could independently extract their line shapes. This minimized the influence that the fits of the electronic transitions had on the frequency and amplitude of the vibrational features.

The transient vibrational spectra obtained from analysis and subtraction of the electronic transitions described above are represented in Figure 3a for each oleate capped PbS QD film for all nanocrystal diameters. The spectra were measured at 20 ns time delay and are plotted as a double difference in absorption $\Delta\Delta$ Abs in units of μ O.D. because they represent results of subtracting a difference signal from a transient absorption measurement. The shading of the negative-going bleach of the ground state vibrational features and the positivegoing transient absorption features match the shading in Figure 2 prior to subtraction of the electronic transition. Because we did not fit the broad electronic transition in the region of the vibrational features appearing in Figure 3a, there is some uncertainty in the baseline defining the zero of the $\Delta\Delta$ Abs signal. We added dotted lines in the 3.7 and 4.9 nm PbS QD spectra as guides to the eye to show qualitatively where this uncertainty may have affected the transient vibrational features.

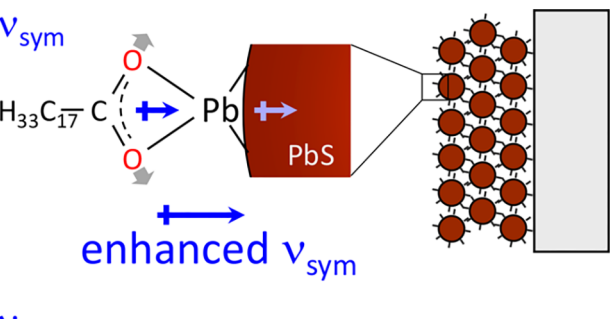
We note that the conclusions of the manuscript are unchanged if we do not follow these guides to the eye. They are included for purposes of visual clarity.

The transient vibrational spectra in Figure 3a are plotted above the FTIR spectrum of the 2.9 nm PbS QD film for comparison. Vertical lines in the FTIR spectrum mark the frequencies of the $\nu_{\rm sym}$ and $\nu_{\rm as}$ carboxylate stretch modes of the chelating structure around 1420 and 1520 cm $^{-1}$, and of the bridging structure around 1400 and 1550 cm $^{-1}$, respectively. These are the same frequencies marked in the FTIR spectra represented in Figure 1. Vertical lines are also included as guides to the eye to mark where the double-bonded C=O and single-bonded C=O moieties absorb with frequencies $\nu_{\rm C=O}$ and $\nu_{\rm C-O}$ around 1600 and 1250 cm $^{-1}$, respectively.

The pattern of frequencies and amplitudes of the transient vibrational features measured in the PbS QD films reveal complementary information about the changes in bonding of oleate ligands to the PbS QD surfaces following optical excitation. For example, a prominent negative-going vibrational feature overlaps the $\nu_{\rm sym}$ and $\nu_{\rm as}$ stretch modes of carboxylate groups involved in the chelating bonding geometry (marked by vertical lines at 1420 and 1520 cm⁻¹). The negative-going feature also overlaps the vibrational features of chelating carboxylate groups in lead-oleate complexes observed in Raman spectra that has been observed around 1450 cm⁻¹.57 Such Raman active vibrational modes can contribute to vibrational features in transient absorption spectra when the vibrational and electronic coordinates are coupled, giving rise to what have been called infrared activated vibrational (IRAV) modes.^{58,59} Such interactions produce negative-going features that interfere with broad electronic absorptions such as those observed in the PbS QD films. We therefore assign the negative-going feature around 1450 cm⁻¹ in the transient vibrational spectra to chelating carboxylic groups interacting with surface lead atoms that are perturbed in the excited electronic state of the PbS QDs.

On either side of the negative-going vibrational feature are transient absorptions that overlap the $\nu_{\rm sym}$ stretch of the bridging geometry around 1400 cm $^{-1}$ and a combination of the $\nu_{\rm as}$ stretch of the bridging and the C=O stretch of the monodentate geometries at 1550 and 1600 cm $^{-1}$, respectively. The amplitudes of the excited state vibrational features of carboxylate groups indicate a pronounced enhancement of their lower frequency symmetric stretch $\nu_{\rm sym}$ and a decreased amplitude of their antisymmetric stretch $\nu_{\rm as}$ modes. The ratio of these peaks differs markedly from their ratio in the FTIR spectrum. Three possible explanations present themselves. The first is simply that the negative-going vibrational feature may have greater overlap with the higher frequency antisymmetric stretch mode and so mask it by cancelation of the oppositely charged features.

The second possibility is that the localization of charge carriers near the QD surfaces in the excited state may modulate the absorption intensity of the vibrational modes as has been observed when carboxylate groups interact with polarizable charge distributions on metal surfaces. Figure 4 illustrates the interactions that could modulate the absorption intensity. The symmetric motion of the carboxylate stretch $\nu_{\rm sym}$ mode causes its transition dipole moment to interact constructively with its image dipole created in the polarizable charge distribution. This can lead to an enhancement of the oscillator strength of the lower frequency $\nu_{\rm sym}$ as observed in the spectra. In contrast, the transition dipole moment of the antisymmetric stretch $\nu_{\rm as}$



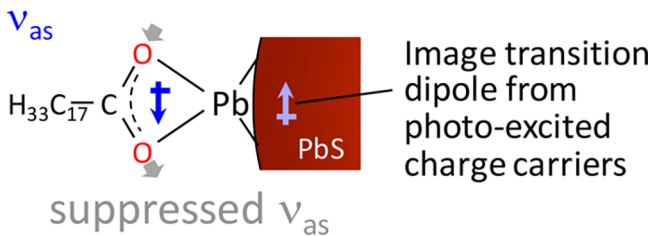


Figure 4. Carboxylate symmetric stretch $\nu_{\rm sym}$ mode creates a transition dipole moment that is reinforced by its image dipole from the polarizable charge distribution near the surfaces of PbS QDs in their excited state. In contrast, the antisymmetric stretch $\nu_{\rm as}$ mode is suppressed due to antiparallel alignment of its image dipole.

mode with its image dipole is destructive, which can reduce its oscillator strength.

A third possible explanation is that the transient features arise from the vibrational Stark effect⁶¹ caused by a change in charge distribution in the excited electronic state. The amplitude of Stark shifted vibrational features depend on their line widths with narrower features exhibiting larger amplitudes. Typical vibrational Stark shifts have been reported in the few cm⁻¹ range. While we cannot eliminate possible contributions from the vibrational Stark effect, it would be surprising to observe such shifts of vibrational features spanning a 300 cm⁻¹ range. We therefore conclude that the vibrational features in Figure 3a arise from some combination of interfering positive and negative vibrational features and screening of the vibrational modes by a polarizable charge distribution in the excited state.

Finally, we note the appearance of a transient vibrational feature around 1250 cm⁻¹ that is indicative of the formation of carboxylate groups in the monodentate bonding geometry. This evidence combined with the preferential perturbation of carboxylates in the chelating geometry (negative-going feature at 1450 cm⁻¹) and the enhancement of the bridging geometry ν_{sym} and ν_{as} modes reveals a net reduction of the Pb-O coordination in the excited excitonic state of PbS QDs in comparison to the ground electronic state. This shift toward lower Pb-O coordination in the excited electronic state is represented in Figure 3b. The chelating bonding geometry involves coordination of both oxygen atoms of the carboxylate groups to individual lead atoms on the QD surfaces. The shift toward more bridging bonding geometries causes the associated lead atoms to be coordinated by only one oxygen atom. The shift to the monodentate geometry reduces the total number of oxygen atoms coordinated to the QD surfaces, leading to a further decrease of the average Pb-O coordination.

These changes of the oleate bonding geometries in the excited excitonic states of PbS QDs are consistent with prior measurements of electrons interacting with ligand—nanocrystal

surface states. 20,62,63 The PbS QDs were synthesized under conditions that lead to lead-rich surfaces. Therefore, localization of electrons at the ligand—nanocrystal surfaces in the excited state would be expected to increase electron density in the antibonding π orbital between the carboxylate and lead atoms in the chelating bonding geometry, weakening the average Pb—O bond strength. We speculate that this is the origin of the decreased Pb—O coordination observed in the transient vibrational spectra. We note that CdS and CdSe QDs and nanorods synthesized using different procedures have been shown to trap holes rather than electrons at their surfaces. If holes were trapped at the lead-rich surfaces of the PbS QDs examined here, we would anticipate an associated strengthening of the carboxylate bonding to the more electro-positive lead atoms.

The dynamic excited state surface chemistry observed here has implications for the use of QDs as photosensitizers in light harvesting and photocatalytic reactions. For example, some applications of nanocrystals in photocatalytic systems utilize them as photoreceptors that transfer electrons to redox shuttles such as viologens 29,30 for subsequent transport of reduction equivalents to the catalyst in the system. 31-33 Other applications use QDs as photocatalysts to oxidize or reduce substrates that approach their surfaces to enable radical—radical reactions. 34-38 Such charge transfer processes are found to be mediated by penetration of the redox shuttle within the ligand shell of the nanocrystals. The ability of small molecular species to penetrate the ligand shell of QDs to undergo such charge transfer processes is influenced by the permeability of the ligand layer that in turn depends on the binding of the surface active functional group to the QD surface.²⁸ It will be interesting to examine nanocrystals having different surface compositions and different exposed crystal facets 66,67 using TRIR spectroscopy in order to better understand how changes in surface chemistry of their excited electronic states may influence their charge transfer and photocatalytic reactivity.

In summary, we investigated the changes in surface chemistry of oleate ligands on PbS quantum dot surfaces following optical excitation of the quantum dots to their excitonic excited states. TRIR spectroscopy directly probed the surface bonding geometries of carboxylate groups of oleate ligands through the time-evolution of their vibrational frequencies. The data revealed a net reduction of the Pb-O coordination of carboxylate groups to lead atoms on the quantum dots surfaces in the excited states of the nanocrystals. In the ground electronic state, oleate ligands bind primarily through chelating and bridging geometries to lead atoms. In the excited state, a net reduction of the more highly coordinated chelating geometry is observed with an associated increase of the bridging and monodentate bonding geometries. These changes are consistent with localization of electrons at the nanocrystal surfaces resulting in a net reduction of the lead atoms in the excited electronic state of the quantum dots. The ability to directly probe ligand-nanocrystal interactions in excited electronic states using TRIR spectroscopy offers the opportunity to investigate the molecular dynamics that influence energy and charge transfer processes at quantum dot surfaces that underpin their use in optoelectronic and photocatalytic applications.

ASSOCIATED CONTENT

Supporting Information

The Supporting Information is available free of charge at https://pubs.acs.org/doi/10.1021/acs.jpclett.0c00539.

Detailed experimental methods, UV-vis and TEM characterization of PbS quantum dot sizes, and Fourier transform infrared spectra of oleate capped PbS quantum dot films (PDF)

AUTHOR INFORMATION

Corresponding Author

John B. Asbury — Magnitude Instruments, State College, Pennsylvania 16803, United States; Department of Chemistry and Intercollege Materials Science and Engineering Program, The Pennsylvania State University, University Park, Pennsylvania 16802, United States; Occid.org/0000-0002-3641-7276; Email: jasbury@psu.edu

Authors

Eric R. Kennehan – Magnitude Instruments, State College, Pennsylvania 16803, United States

Kyle T. Munson – Department of Chemistry, The Pennsylvania State University, University Park, Pennsylvania 16802, United States

Grayson S. Doucette — Intercollege Materials Science and Engineering Program and Department of Materials Science and Engineering, The Pennsylvania State University, University Park, Pennsylvania 16802, United States

Ashley R. Marshall — Chemical and Materials Science, National Renewable Energy Laboratory (NREL), Golden, Colorado 80401, United States; Department of Chemistry and Biochemistry, University of Colorado, Boulder, Colorado 80309, United States

Matthew C. Beard — Chemical and Materials Science, National Renewable Energy Laboratory (NREL), Golden, Colorado 80401, United States; Department of Chemistry and Biochemistry, University of Colorado, Boulder, Colorado 80309, United States; Ocid.org/0000-0002-2711-1355

Complete contact information is available at: https://pubs.acs.org/10.1021/acs.jpclett.0c00539

Notes

The authors declare the following competing financial interest(s): E.R.K. and J.B.A. own equity in Magnitude Instruments, which has an interest in this project. Their ownership in this company has been reviewed by the Pennsylvania State University Individual Conflict of Interest Committee and is currently being managed by the University.

■ ACKNOWLEDGMENTS

E.R.K. recognizes partial support of this research from Magnitude Instruments. G.S.D. and J.B.A. thank the U.S. Department of Energy (DOE), Office of Science, Office of Basic Energy Sciences for support of this research through Grant DE-SC0019349. K.T.M. is grateful for support from the National Science Foundation Graduate Research Fellowship Program under Grant DGE1255832. A.R.M. and M.C.B. acknowledge support from the solar photochemistry program within the Division of Chemistry, Geosciences and Biosciences, Office of Basic Energy Sciences, Office of Science within the U.S. DOE. Part of this work was authored by the Alliance for Sustainable Energy, LLC, the manager and

operator of the National Renewable Energy Laboratory for DOE under Contract DE-AC36-08GO28308.

REFERENCES

- (1) Pietryga, J. M.; Park, Y.-S.; Lim, J.; Fidler, A. F.; Bae, W. K.; Brovelli, S.; Klimov, V. I. Spectroscopic and Device Aspects of Nanocrystal Quantum Dots. *Chem. Rev.* **2016**, *116*, 10513–10622.
- (2) Nozik, A. J.; Beard, M. C.; Luther, J. M.; Law, M.; Ellingson, R. J.; Johnson, J. C. Semiconductor Quantum Dots and Quantum Dot Arrays and Applications of Multiple Exciton Generation to Third-Generation Photovoltaic Solar Cells. *Chem. Rev.* **2010**, *110*, 6873–6890.
- (3) Beard, M. C.; Luther, J. M.; Nozik, A. J. The Promise and Challenge of Nanostructured Solar Cells. *Nat. Nanotechnol.* **2014**, *9*, 951–954.
- (4) Bera, D.; Qian, L.; Tseng, T.-K.; Holloway, P. H. Quantum Dots and Their Multimodal Applications: A Review. *Materials* **2010**, *3*, 2260–2345.
- (5) Kramer, I.; Sargent, E. H. The Architecture of Colloidal Quantum Dot Solar Cells: Materials to Devices. *Chem. Rev.* **2014**, 114, 863–882.
- (6) Konstantatos, G.; Sargent, E. H. Pbs Colloidal Quantum Dot Photoconductive Photodetectors: Transport, Traps, and Gain. *Appl. Phys. Lett.* **2007**, *91*, 173505–1–173505–3.
- (7) Ruhle, S. Tabulated Values of the Shockley-Queisser Limit for Single Junction Solar Cells. *Sol. Energy* **2016**, *130*, 139–147.
- (8) Ellingson, R. J.; Beard, M. C.; Johnson, J. C.; Yu, P.; Micic, O. I.; Nozik, A. J.; Shabaev, A.; Efros, A. L. Highly Efficient Multiple Exciton Generation in Colloidal Pbse and Pbs Quantum Dots. *Nano Lett.* **2005**, *5*, 865–871.
- (9) Luther, J. M.; Beard, M. C.; Song, Q.; Law, M.; Ellingson, R. J.; Nozik, A. J. Multiple Exciton Generation in Films of Electronically Coupled Pbse Quantum Dots. *Nano Lett.* **2007**, *7*, 1779–1784.
- (10) Semonin, O. E.; Luther, J. M.; Choi, S.; Chen, H.-Y.; Gao, J.; Nozik, A. J.; Beard, M. C. Peak External Photocurrent Quantum Efficiency Exceeding 100% Via Meg in a Quantum Dot Solar Cell. *Science* **2011**, 334, 1530–1533.
- (11) Beard, M. C.; Johnson, J. C.; Luther, J. M.; Nozik, A. J. Multiple Exciton Generation in Quantum Dots Versus Singlet Fission in Molecular Chromophores for Solar Photon Conversion. *Philos. Trans. R. Soc., A* **2015**, 373, 20140412.
- (12) Midgett, A. G.; Luther, J. M.; Stewart, J. T.; Smith, D. K.; Padilha, L. A.; Klimov, V. I.; Nozik, A. J.; Beard, M. C. Size and Composition Dependent Multiple Exciton Generation Efficiency in Pbs, Pbse, and Pbs(X)Se(1-X) Alloyed Quantum Dots. *Nano Lett.* **2013**, *13*, 3078–3085.
- (13) Pandey, A.; Guyot-Sionnest, P. Hot Electron Extraction from Colloidal Quantum Dots. *J. Phys. Chem. Lett.* **2010**, *1*, 45–47.
- (14) Cho, B.; Peters, W. K.; Hill, R. J.; Courtney, T. L.; Jonas, D. M. Bulklike Hot Carrier Dynamics in Lead Sulfide Quantum Dots. *Nano Lett.* **2010**, *10*, 2498–2505.
- (15) Schaller, R. D.; Pietryga, J. M.; Goupalov, S. V.; Petruska, M. A.; Ivanov, S. A.; Klimov, V. I. Breaking the Phonon Bottleneck in Semiconductor Nanocrystals Via Multiphonon Emission Induced by Intrinsic Nonadiabatic Interactions. *Phys. Rev. Lett.* **2005**, *95*, 196401.
- (16) El-Ballouli, A. a. O.; Alarousu, E.; Usman, A.; Pan, J.; Bakr, O. M.; Mohammed, O. F. Real-Time Observation of Ultrafast Intraband Relaxation and Exciton Multiplication in Pbs Quantum Dots. ACS Photonics 2014, 1, 285–292.
- (17) Cooney, R. R.; Sewall, S. L.; Anderson, K. E. H.; Dias, E. A.; Kambhampati, P. Breaking the Phonon Bottleneck for Holes in Semiconductor Quantum Dots. *Phys. Rev. Lett.* **2007**, *98*, 177403.
- (18) Cooney, R. R.; Sewall, S. L.; Dias, E. A.; Sagar, D. M.; Anderson, K. E. H.; Kambhampati, P. Unified Picture of Electron and Hole Relaxation Pathways in Semiconductor Quantum Dots. *Phys. Rev. B: Condens. Matter Mater. Phys.* **2007**, *75*, 245311.
- (19) Pandey, A.; Guyot-Sionnest, P. Slow Electron Cooling in Colloidal Quantum Dots. *Science* **2008**, 322, 929–932.

- (20) Guyot-Sionnest, P.; Wehrenberg, B.; Yu, D. Intraband Relaxation in Cdse Nanocrystals and the Strong Influence of the Surface Ligands. *J. Chem. Phys.* **2005**, 123, 074709.
- (21) Liu, H.; Guyot-Sionnest, P. Photoluminescence Lifetime of Lead Selenide Colloidal Quantum Dots. J. Phys. Chem. C 2010, 114, 14860–14863.
- (22) Kambhampati, P. Unraveling the Structure and Dynamics of Excitons in Semiconductor Quantum Dots. *Acc. Chem. Res.* **2011**, *44*, 1–13
- (23) Lifshitz, E. Evidence in Support of Exciton to Ligand Vibrational Coupling in Colloidal Quantum Dots. *J. Phys. Chem. Lett.* **2015**, *6*, 4336–4347.
- (24) Mack, T. G.; Jethi, L.; Andrews, M.; Kambhampati, P. Direct Observation of Vibronic Coupling between Excitonic States of Cdse Nanocrystals and Their Passivating Ligands. *J. Phys. Chem. C* **2019**, 123, 5084–5091.
- (25) Schnitzenbaumer, K. J.; Dukovic, G. Comparison of Phonon Damping Behavior in Quantum Dots Capped with Organic and Inorganic Ligands. *Nano Lett.* **2018**, *18*, 3667–3674.
- (26) Mack, T. G.; Jethi, L.; Kambhampati, P. Temperature Dependence of Emission Line Widths from Semiconductor Nanocrystals Reveals Vibronic Contributions to Line Broadening Processes. J. Phys. Chem. C 2017, 121, 28537—28545.
- (27) Kennehan, E. R.; Doucette, G. S.; Marshall, A. R.; Grieco, C.; Munson, K. T.; Beard, M. C.; Asbury, J. B. Electron-Phonon Coupling and Resonant Relaxation from 1d and 1p States in Pbs Quantum Dots. *ACS Nano* **2018**, *12*, 6263–6272.
- (28) Malicki, M.; Knowles, K. E.; Weiss, E. A. Gating of Hole Transfer from Photoexcited Pbs Quantum Dots to Aminoferrocene by the Ligand Shell of the Dots. *Chem. Commun.* **2013**, *49*, 4400–4402.
- (29) Boldt, K.; Jander, S.; Hoppe, K.; Weller, H. Characterization of the Organic Ligand Shell of Semiconductor Quantum Dots by Fluorescence Quenching Experiments. *ACS Nano* **2011**, *5*, 8115–8123.
- (30) Morris-Cohen, A. J.; Vasilenko, V.; Amin, V. A.; Reuter, M. G.; Weiss, E. A. Model for the Adsorption of Ligands to Colloidal Quantum Dots with Concentration-Dependent Surface Structure. *ACS Nano* **2012**, *6*, 557–565.
- (31) Wu, H.; Zhu, H.; Lian, T. Ultrafast Exciton Dynamics and Light-Driven H2 Evolution in Colloidal Semiconductor Nanorods and Pt-Tipped Nanorods. *Acc. Chem. Res.* **2015**, *48*, 851–859.
- (32) Harris, C.; Kamat, P. V. Photocatalytic Events of Cdse Quantum Dots in Confined Media. Electodic Behavior of Coupled Platinum Nanoparticles. *ACS Nano* **2010**, *4*, 7321–7330.
- (33) Sanchez, M. L. K.; Wu, C.-H.; Adams, M. W. W.; Dyer, R. B. Optimizing Electron Transfer from Cdse Qds to Hydrogenase for Photocatalytic H2 Production. *Chem. Commun.* **2019**, *55*, 5579–5582.
- (34) Caputo, J. A.; Frenette, L. C.; Zhao, N.; Sowers, K. L.; Krauss, T. D.; Weix, D. J. General and Efficient C-C Bond Forming Photoredox Catalysis with Semiconductor Quantum Dots. *J. Am. Chem. Soc.* **2017**, *139*, 4250–4253.
- (35) Zhang, Z.; Edme, K.; Lian, S.; Weiss, E. A. Enhancing the Rate of Quantum-Dot-Photocatalyzed Carbon-Carbon Coupling by Tuning the Composition of the Dot's Ligand Shell. *J. Am. Chem. Soc.* 2017, 139, 4246–4249.
- (36) Zhu, X.; Lin, Y.; Sun, Y.; Beard, M. C.; Yan, Y. Lead-Halide Perovskites for Photocatalytic a-Alkylation of Aldehydes. *J. Am. Chem. Soc.* **2019**, *141*, 733–738.
- (37) Wang, K.; Lu, H.; Zhu, X.; Lin, Y.; Beard, M. C.; Yan, Y.; Chen, X. Ultrafast Reaction Mechanisms in Perovskite Based Photocatalytic C-C Coupling. ACS Energy Lett. **2020**, *5*, 566–571.
- (38) Lu, H.; Zhu, X.; Miller, C.; San Martin, J.; Chen, X.; Miller, E. M.; Yan, Y.; Beard, M. C. Enhanced Photoredox Activity of Cspbbr3 Nanocrystals by Quantitative Colloidal Ligand Exchange. *J. Chem. Phys.* **2019**, *151*, 204305.

- (39) Frederick, M. T.; Amin, V. A.; Weiss, E. A. Optical Properties of Strongly Coupled Quantum Dot-Ligand Systems. *J. Phys. Chem. Lett.* **2013**, *4*, 634–640.
- (40) Fischer, S. A.; Crotty, A. M.; Kilina, S. V.; Ivanov, S. A.; Tretiak, S. Passivating Ligand and Solvent Contributions to the Electronic Properties of Semiconductor Nanocrystals. *Nanoscale* **2012**, *4*, 904–914.
- (41) Brown, P. R.; Kim, D.; Lunt, R. R.; Zhao, N.; Bawendi, M.; Grossman, J. C.; Bulovic, V. Energy Level Modification in Lead Sulfide Quantum Dot Thin Films through Ligand Exchange. *ACS Nano* **2014**, *8*, 5863–5872.
- (42) Liang, Y.; Thorne, J. E.; Parkinson, B. A. Controlling the Electronic Coupling between Cdse Quantum Dots and Thiol Capping Ligands via pH and Ligand Selection. *Langmuir* **2012**, *28*, 11072—11077.
- (43) Kroupa, D. M.; Voros, M.; Brawand, N. P.; McNichols, B. W.; Miller, E. M.; Gu, J.; Nozik, A. J.; Sellinger, A.; Galli, G.; Beard, M. C. Tuning Colloidal Quantum Dot Band Edge Positions through Solution-Phase Surface Chemistry Modification. *Nat. Commun.* **2017**, *8*, 15257.
- (44) Spoor, F. C. M.; Tomic, S.; Houtepen, A. J.; Siebbeles, L. D. A. Broadband Cooling Spectra of Hot Electrons and Holes in Pbse Quantum Dots. *ACS Nano* **2017**, *11*, 6286–6294.
- (45) Jiang, Y.; Wang, C.; Rogers, C. R.; Kodaimati, M.; Weiss, E. A. Regio- and Diastereoselective Intermolecular [2 + 2] Cycloadditions Photocatalyzed by Quantum Dots. *Nat. Chem.* **2019**, *11*, 1034–1040.
- (46) Munson, K. T.; Kennehan, E. R.; Asbury, J. B. Structural Origins of the Electronic Properties of Materials Via Time-Resolved Infrared Spectroscopy. *J. Mater. Chem. C* **2019**, *7*, 5889–5909.
- (47) Munson, K. T.; Doucette, G. S.; Kennehan, E. R.; Swartzfager, J. R.; Asbury, J. B. Vibrational Probe of the Structural Origins of Slow Recombination in Halide Perovskites. *J. Phys. Chem. C* **2019**, *123*, 7061–7073.
- (48) Munson, K. T.; Kennehan, E. R.; Doucette, G. S.; Asbury, J. B. Dynamic Disorder Dominates Delocalization, Transport, and Recombination in Halide Perovskites. *Chem.* **2018**, *4*, 2826–2843.
- (49) Kennehan, E. R.; Grieco, C.; Brigeman, A. N.; Doucette, G. S.; Rimshaw, A.; Bisgaier, K.; Giebink, N. C.; Asbury, J. B. Using Molecular Vibrations to Probe Exciton Delocalization in Films of Perylene Diimides with Ultrafast Mid-Ir Spectroscopy. *Phys. Chem. Chem. Phys.* **2017**, *19*, 24829–24839.
- (50) Grieco, C.; Kennehan, E. R.; Rimshaw, A.; Payne, M. M.; Anthony, J. E.; Asbury, J. B. Harnessing Molecular Vibrations to Probe Triplet Dynamics During Singlet Fission. *J. Phys. Chem. Lett.* **2017**, *8*, 5700–5706.
- (51) Harris, R. D.; Homan, S. B.; Kodaimati, M.; He, C.; Nepomnyashchii, A. B.; Swenson, N. K.; Lian, S.; Calzada, R.; Weiss, E. A. Electronic Processes within Quantum Dot-Molecule Complexes. *Chem. Rev.* **2016**, *116*, 12865–12919.
- (52) Hines, M. A.; Scholes, G. D. Colloidal Pbs Nanocrystals with Size-Tunable near-Infrared Emission: Observation of Post-Synthesis Self-Narrowing of the Particle Size Distribution. *Adv. Mater.* **2003**, *15*, 1844–1849.
- (53) Cass, L. C.; Malicki, M.; Weiss, E. A. The Chemical Environments of Oleate Species within Samples of Oleate-Coated Pbs Quantum Dots. *Anal. Chem.* **2013**, *85*, 6974–6979.
- (54) Crisp, R. W.; Kroupa, D. M.; Marshall, A. R.; Miller, E. M.; Zhang, J.; Beard, M. C.; Luther, J. M. Metal Halide Solid-State Surface Treatment for High Efficiency Pbs and Pbse QD Solar Cells. *Sci. Rep.* **2015**, *5*, 9945.
- (55) Jeong, K. S.; Tang, J.; Liu, H.; Kim, J.; Schaefer, A. W.; Kemp, K.; Levina, L.; Wang, X.; Hoogland, S.; Debnath, R.; Brzosowski, L.; Sargent, E. H.; Asbury, J. B. Enhanced Mobility-Lifetime Products in Pbs Colloidal Quantum Dot Photovoltaics. *ACS Nano* **2012**, *6*, 89–99.
- (56) Deacon, G. B.; Phillips, R. J. Relationships between the Carbon-Oxygen Stretching Frequencies of Carboxylato Complexes and the Type of Carboxylate Coordination. *Coord. Chem. Rev.* **1980**, 33, 227–250.

- (57) Otero, V.; Sanches, D.; Montagner, C.; Vilarigues, M.; Carlyle, L.; Lopes, J. A.; Melo, M. J. Characterization of Metal Carboxylates by Raman and Infrared Spectroscopy in Works of Art. *J. Raman Spectrosc.* **2014**, *45*, 1197–1206.
- (58) Kim, Y. H.; Foster, C. M.; Heeger, A. J. Polarons in High Tc Superconductors: Irav Modes and Electronic Transitions to Gap States as in Conducting Polymers. *Synth. Met.* **1989**, *29*, F603–F608.
- (59) Miranda, P. B.; Moses, D.; Heeger, A. J. Ultrafast Photogeneration of Charged Polarons in Conjugated Polymers. *Phys. Rev. B: Condens. Matter Mater. Phys.* **2001**, *64*, 081201.
- (60) Wulandari, P.; Nagahiro, T.; Fukada, N.; Kimura, Y.; Niwano, M.; Tamada, K. Characterization of Citrates on Gold and Silver Nanoparticles. *J. Colloid Interface Sci.* **2015**, 438, 244–248.
- (61) Boxer, S. G. Stark Realities. J. Phys. Chem. B 2009, 113, 2972-
- (62) Turk, M. E.; Vora, P. M.; Fafarman, A. T.; Diroll, B. T.; Murray, C. B.; Kagan, C. R.; Kikkawa, J. M. Ultrafast Electron Trapping in Ligand-Exchanged Quantum Dot Assemblies. *ACS Nano* **2015**, *9*, 1440–1447.
- (63) Boehme, S. C.; Walvis, T. A.; Infante, I.; Grozema, F. C.; Vanmaekelbergh, D.; Siebbeles, L. D. A.; Houtepen, A. J. Electrochemical Control over Photoinduced Electron Transfer and Trapping in Cdse-Cdte Quantum-Dot Solids. *ACS Nano* **2014**, *8*, 7067–7077.
- (64) Wuister, S. F.; de Mello Donega, C.; Meijerink, A. Influence of Thiol Capping on the Exciton Luminescence and Decay Kinetics of Cdte and Cdse Quantum Dots. *J. Phys. Chem. B* **2004**, *108*, 17393–17397.
- (65) Wu, H.; Zhu, H.; Liu, Z.; Rodriguez-Cordoba, W.; Lian, T. Ultrafast Charge Separation and Long-Lived Charge Separated State in Photocatalytic Cds-Pt Nanorod Heterostructures. *J. Am. Chem. Soc.* **2012**, *134*, 10337–10340.
- (66) Rao, S. S.; Durga, I. K.; Tulasi-Varma, C. V.; Punnoose, D.; Cheol, L. J.; Kim, H.-J. The Synthesis and Characterization of Lead Sulfide with Cube-Like Structure as a Counter Electrode in the Presence of Urea Using a Hydrothermal Method. *New J. Chem.* **2015**, 39, 7379–7388.
- (67) Choi, H.; Ko, J.-H.; Kim, Y.-H.; Jeong, S. Steric-Hindrance-Driven Shape Transition in Pbs Quantum Dots: Understanding Size-Dependent Stability. *J. Am. Chem. Soc.* **2013**, *135*, 5278–5281.